coatings

MDPI

Article

Research on Wear and Corrosion Resistance of Ni60-WC Coating Fabricated by Laser on the Preheated Copper Alloy

Yu Liu [1,2,*], Tianhao Xu [1] and Guohui Li [2]

[1] School of Mechanical Engineering, Northeast Electric Power University, No. 169 Changchun Road, Chuanying District, Jilin 132012, China
[2] International Shipping Research Institute, Gongqing Institute of Science and Technology, Gongqing 332020, China
* Correspondence: yuliu@neepu.edu.cn

Abstract: The copper alloy is widely used to prepare pipes in ocean engineering. The surface is washed and corroded by seawater for a long time, which gradually shortens the service life of the condenser tube. In order to improve the wear and corrosion resistance of copper alloy, a Ni60-WC coating was fabricated on a preheated copper alloy by laser cladding. Experiments on the Ni60-WC coatings were carried out by SEM, XRD, Vickers-microhardness meter, wear tester and electrochemical workstation. The microstructure, phases, hardness, wear and corrosion resistance were investigated. The results show that from the top to bottom, the microstructures were columnar dendrites, dendritic crystals and grains, respectively. The wear rate of the Ni60-WC coating was only 4.9×10^{-5} mm^3·N^{-1}·m^{-1}, which was only 1.14% of copper substrate. In addition, the corrosion current density was 2.34×10^{-7} mA·mm^{-2}, which was much lower than that of copper alloy substrate (1.14×10^{-6} mA·mm^{-2}). The experimental results show that this Ni60-WC coating has a good metallurgical bonding and hardness, and it also has good wear and corrosion resistance, which is helpful to improve the service life of the condenser tube.

Keywords: laser cladding; copper alloy; coating; microstructure; wear resistance; electrochemical corrosion

Citation: Liu, Y.; Xu, T.; Li, G. Research on Wear and Corrosion Resistance of Ni60-WC Coating Fabricated by Laser on the Preheated Copper Alloy. *Coatings* **2022**, *12*, 1537. https://doi.org/10.3390/coatings12101537

Academic Editor: Armando Yáñez-Casal

Received: 9 September 2022
Accepted: 10 October 2022
Published: 13 October 2022

1. Introduction

The copper alloy is widely used in the mechanical manufacture of pipes due to its good corrosion resistance and fatigue strength [1–3]. However, failure sometimes occurs during the long service, which reduces the service life of copper alloy [4]. In order to reduce accidents, some surface modification technologies are used to fabricate coatings, such as laser cladding [5], electrophoretic deposition [6,7] and thermal spraying [8]. In the past decades, laser cladding has been widely used to fabricate coating due to its advantages of high efficiency and low cost [9–11].

Due to the high thermal conductivity and reflectivity of copper alloy [12], the coating obtained by laser cladding usually has poor bonding [13] and some defects [14] with copper alloy. In order to solve these problems, researchers have prepared Ni-based [15], Co-based [16] and Fe-based [17] coatings on the surface of copper alloys. The Ni-based alloy powder is considered to be a preferred material [18–20]. However, the wear resistance and corrosion resistance of simple Ni-based alloy coating are not suitable for some harsh working environments [21,22].

It is an effective method to improve the performance of Ni-based coatings by adding reinforced ceramic particles [23]. The ceramic particles mainly include oxides [24], carbides [25], silicides [26], borides [27] and nitrides [28] of transition metal elements. Among these ceramic phases, WC has a high melting point, high hardness, a low thermal expansion coefficient and good wettability with nickel-based alloys [29]. WC is the most widely used in laser cladding particle reinforced Ni-based coatings [30]. However, WC is easy to

decompose some secondary precipitates such as block, strip or layered carbides at high temperatures. These secondary precipitates are easy to bring some cracks to the coating [31]. In order to slow down heat transfer, a new method with preheating temperature was proposed to increase the coating's properties and decrease the coating's defects.

In this paper, a Ni60-WC coating was designed and fabricated by laser on preheated copper alloy. The microstructure and properties were studied by the SEM, EDS, XRD and electrochemical workstation. The performance of the Ni60-WC coating was greatly improved, which provided a reference for preparing the coating on the copper alloy substrate.

2. Materials and Methods

2.1. Materials

The aluminum brass was selected as the substrate, and the size was 50 mm × 30 mm × 10 mm. The fouling and oxide on the surface were removed by a grinding and polishing machine. The coating material is an Ni-based alloy powder with an average size of 35−150 μm. The composite of copper alloy and Ni60-WC alloy powders are included in Tables 1 and 2, respectively. The physical and mechanical characteristics of the copper alloy are included in Table 3.

Table 1. The composite of copper alloy (wt.%).

Material	Fe	Mn	Al	Zn	Cu
Copper alloy	1.35	3.2	6.3	29.01	60.14

Table 2. The composite of Ni60-WC alloy powder (wt.%).

Material	Ni	WC	Cr	Si	B	C	Fe
Ni60-WC powder	66	5	12	1.5	2.5	1	12

Table 3. Physical and mechanical characteristics of copper alloy.

Property	Copper Alloys
Density	7281.32 $kg{\cdot}m^{-3}$
Specific Heat	468.2 $J{\cdot}(kg{\cdot}^{\circ}C)^{-1}$
Thermal conductivity	61.74 $W{\cdot}(m{\cdot}K)^{-1}$
Thermal expansion coefficient	23.58×10^{-6}
Young's modulus	87.07 MPa
Resistivity	0.071×10^{-6} $\Omega{\cdot}m^{-1}$

2.2. Methods

Figure 1 shows the schematic diagram and the actual operation of the laser cladding process on the preheated copper alloy. The parameters of the laser system (DL-HL-T2000, Shenyang DALU Laser Technology Co., Ltd., Shenyang, China) were as follows: laser power 1.4 kW, laser beam diameter 3.0 mm, scanning speed 2 $mm{\cdot}s^{-1}$ and overlapping ratio 30%, as shown in Table 4. The preheating temperature was 200 °C. The nozzle was controlled by CNC numerical control device. The coating after laser cladding was cut into five 10 mm × 10 mm × 10 mm samples. After the samples were buffed and polished, a ferric chloride solution was used to etch the cladding coating for 10 s. Then, the samples were observed by optical microscopy and scanning election microscopy (TESCAN MIRA, TESCAN, Brno, Czech Republic). The acceleration voltage of scanning election microscopy was 20 kV and the working depth of scanning election microscopy was 8 mm. At the same time, the element distribution was analyzed by EDS (TESCAN MIRA, TESCAN, Brno, Czech Republic). Four EDS tests were carried out to reduce errors. The phases are detected by X-ray diffraction (TD-3500, Dandong Tongda Science and Technology Co., Ltd., Dandong, China).

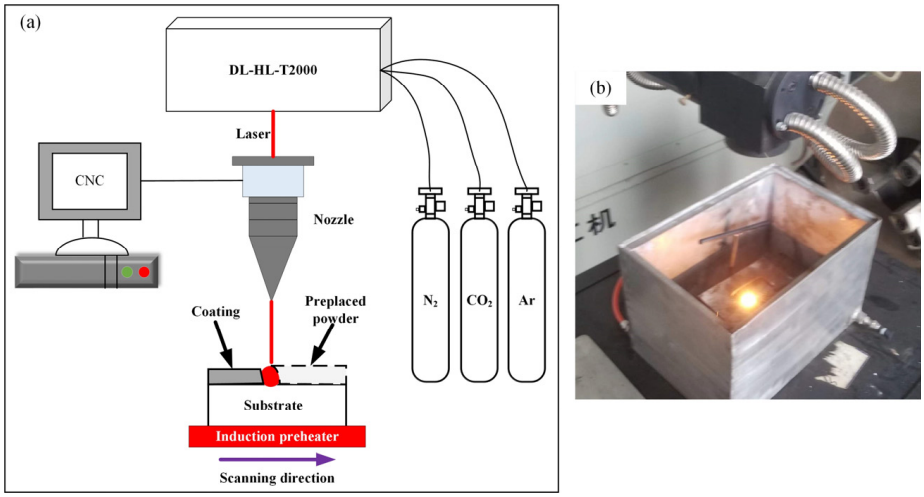

Figure 1. Schematic diagram (**a**) and the actual operation (**b**) of laser cladding process on the preheated copper alloy.

Table 4. Process parameters of laser cladding.

Process Parameters	Value
Laser power	1400 W
Scanning speed	2 mm·s^{-1}
Preheating temperature	200 °C
Laser beam diameter	3 mm
Overlap rate	30%

The microhardness was tested by Vickers microhardness meter (HXD-1000TMC/LCD, Shanghai Optical Instrument Co., Ltd., Shanghai, China) with a load of 50 gf at 15 s. The positive pyramid diamond indenter was used to press the sample surface under the action of the test force. After maintaining the specified time, the test force was removed and the diagonal length of the indentation on the sample surface was measured. Figure 2 is the microhardness test diagram of coating. The microhardness measuring points were uniformly located in the 5 × 22 lattices on the cross section of the specimen, where 5 × 16 lattices were located in the coating, 5 × 3 lattices in the interface, and 3 × 3 lattices in the copper alloy substrate. The distance between adjacent horizontal points was 0.03 mm. The microhardness was measured from the top of the Ni60-WC coating to copper alloy substrate, and each point was repeated five times at the same height.

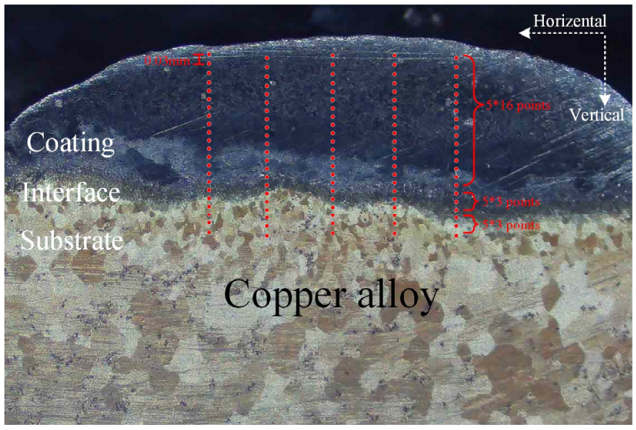

Figure 2. The microhardness test diagram of coating.

The wear property was tested using a reciprocating fatigue wear tester (MGW-02, Jinan Yihua Tribology Testing Technology Co., Ltd., Jinan, China) with a tip force of 10 N and friction frequency 2 Hz. Before the experiment, the surface of the sample cladding coating was polished to a certain extent. Friction mode was the spherical-plane type of dry sliding reciprocating friction. The grinding ball with the size of Φ0.65 mm was selected as the friction pair of cladding coating.

The experiment of electrochemical corrosion was also carried out to investigate the corrosion resistance. The electrochemical workstation software was CHI660E (Shanghai Chenhua Instrument Co., Ltd., Shanghai, China). Electrochemical experiments were performed at room temperature (25 °C). The 3.5% NaCl aqueous solution was configured as the corrosion solution and the immersion time was 2 h. Before the experiment, the surface, except the coating test surface, was sealed with epoxy resin. The reference electrode was saturated calomel electrode and auxiliary electrode was platinum wire electrode. The scanning rate was 0.01 V/s and test voltage range was from −1.6 V to 0.8 V. The electrochemical corrosion performance of the coating was analyzed according to the potentiodynamic polarization curve.

3. Results and Discussion

3.1. Morphology and Phases

Figure 3 shows the surface morphology of the Ni60-WC coating. It can be seen that a Ni60-WC coating has been successfully fabricated on the copper alloy substrate. There were some pores on the coating's surface due to the flow of liquid metal in molten pool, but the pores basically disappeared under the coating's surface.

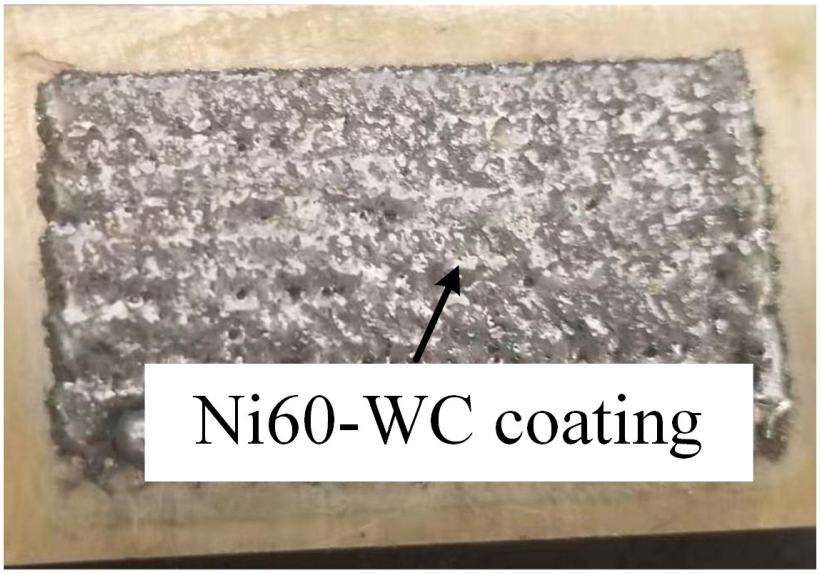

Figure 3. Surface morphology of Ni60-WC coating.

Figure 4 shows the XRD pattern of the Ni60-WC coating surface. The phases are mainly composed of γ (Fe, Ni), WC, W_2C, Ni_3B, Ni_4B_3, $Cr_{0.09}Fe_{0.7}Ni_{0.21}$ and M_7C_3 (M = Fe, Cr). The preheating temperature makes the heat of the molten pool increase, and prolongs the solidification time. The elements, such as Ni, Cr and Fe, have enough time to form reinforced phases.

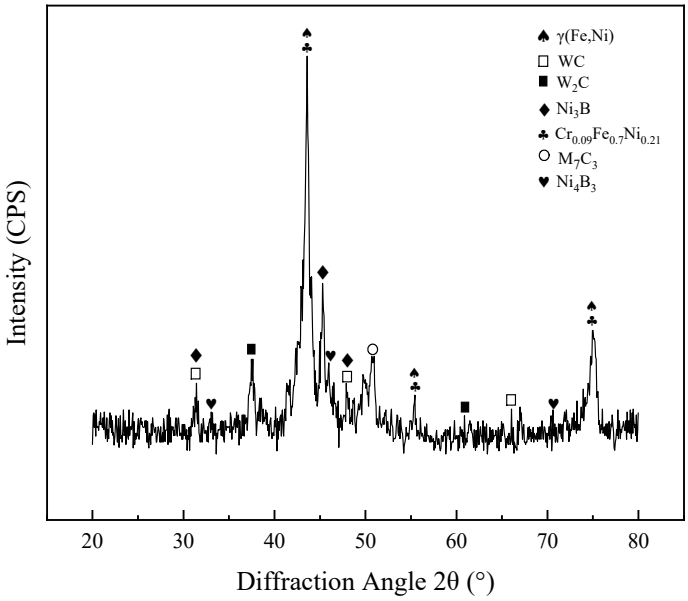

Figure 4. XRD pattern of Ni60-WC coating.

3.2. Microstructure and Binding Region

Figure 5 depicts the cross-section microstructure morphologies of cladding coating. As shown in Figure 5a, the whole cross-section is divided to be three parts, outermost surface, middle and binding region. In Figure 5b, some columnar dendrites forms at the coating's outermost surface due to the quick transfer and it can grow more fully. In Figure 5c, the dendritic crystal is composed of refined dendritic region (DR) and inter dendritic region (IR) in the middle of cladding coating. P_1 point in refined dendritic region is selected for EDS composition detection. At the bottom of cladding coating, some large plane crystals and fine grains forms due to the low heat transfer and cooling rate as shown in Figure 5d.

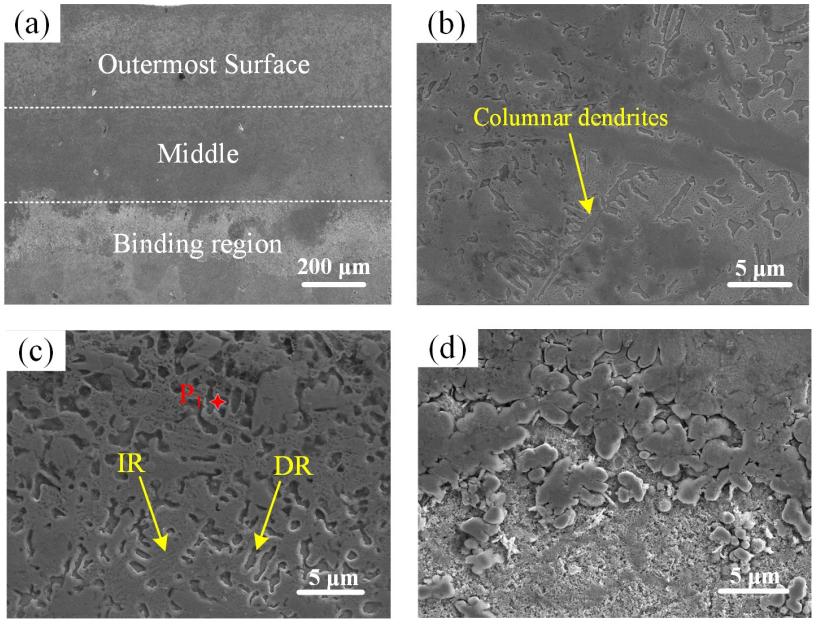

Figure 5. Cross-section microstructure morphologies of cladding coating: (**a**) whole coating; (**b**) outermost surface; (**c**) middle; and (**d**) binding region.

Figure 6 shows the EDS results of P_1 point in the middle of coating. According to the atomic percentage of elements at point P_1, there are a large number of Fe and Ni elements,

which forms a supersaturated solid solution of γ (Fe, Ni) phase. Some C atoms form WC, W_2C, Fe_7C_3 and Cr_7C_3 phases.

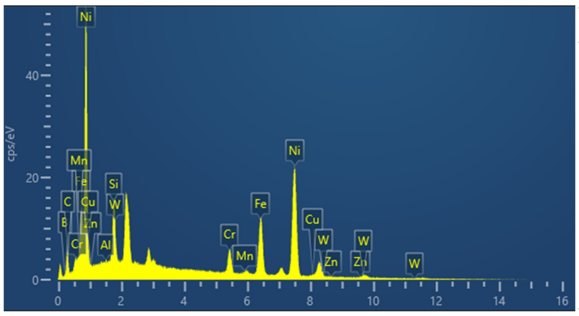

Elements	Atomic concentration %
Ni	39.7
Fe	11.6
C	35.4
W	5.4
B	2.8
Cu	1.7
Zn	-
Cr	3.4

(**a**) (**b**)

Figure 6. EDS results of P_1 point in the middle of coating. (**a**) is element distribution and (**b**) is the proportion of element.

Figure 7 is a SEM micrograph and the distribution of elements in the binding region. It can be seen that the Ni and Fe are uniformly distributed in the binding region, which can obtain a good metallurgical bonding. Meanwhile, M_7C_3 and $Cr_{0.09}Fe_{0.7}Ni_{0.21}$ form due to the appearance of Cr, Fe and Ni.

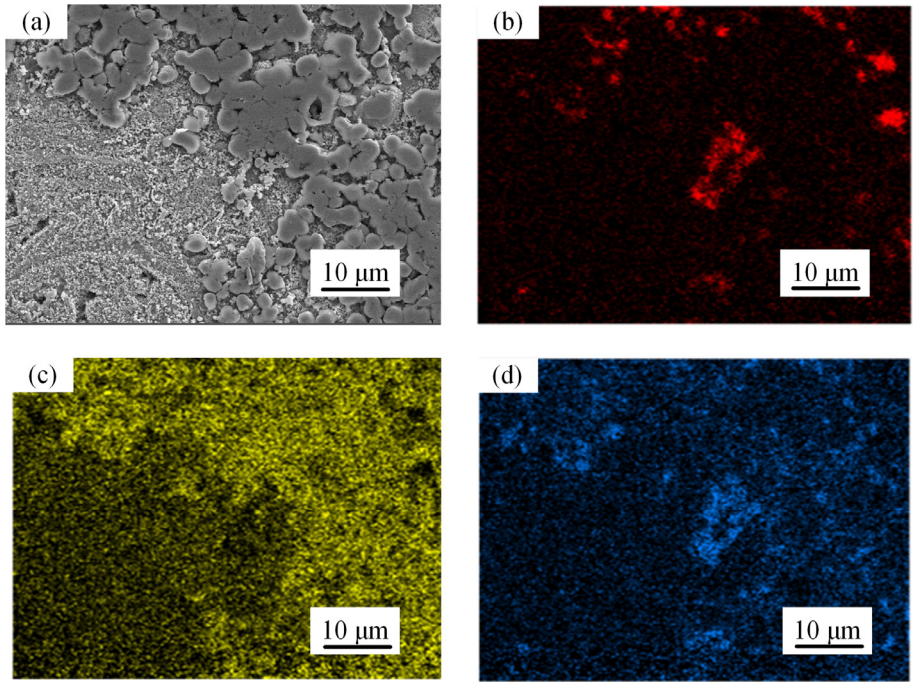

Figure 7. SEM micrograph and distribution of elements in the binding region: (**a**) SEM micrograph; (**b**) element Cr; (**c**) element Ni; and (**d**) element Fe.

3.3. Microhardness

Figure 8 depicts the microhardness of coating from the top to bottom. The maximum and minimum microhardness of the strengthening layer are 1069.3 and 827.2 $HV_{0.5}$. The average microhardness is 941.6 $HV_{0.5}$, which is about 4.7 times greater than that of copper alloy substrate. In the strengthening layer, the change of microhardness is small and smooth, which demonstrates that the strengthening layer has a good quality. This is caused by the uniform distribution of the refined columnar dendrites and dendritic crystal.

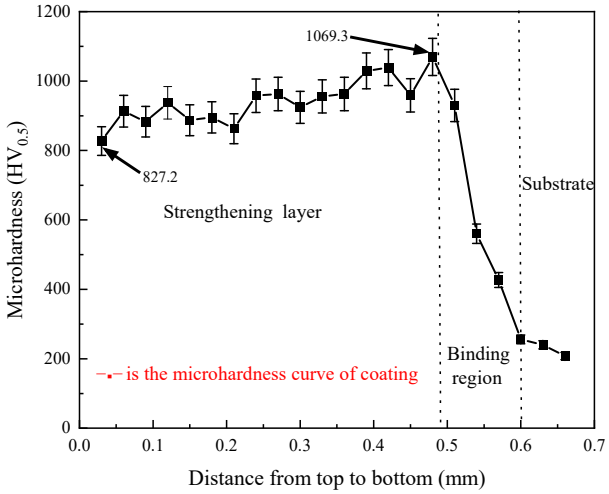

Figure 8. Microhardness of cladding coating from the top to bottom.

3.4. Wear Resistance

The friction experiments are carried out for 30 min. Figure 9 shows the friction coefficient of the Ni60-WC coating and copper substrate. The friction coefficient of copper substrate is stable around 0.18, while the friction coefficient of the Ni60-WC coating has two rapid rises and then stabilized around 0.1, which is slightly lower than the friction coefficient of copper substrate. The existence of reinforced phases makes the friction coefficient unstable and leads to have the rapid rises. Meanwhile, those phases also decrease the friction coefficient and improve the wear resistance of copper substrate.

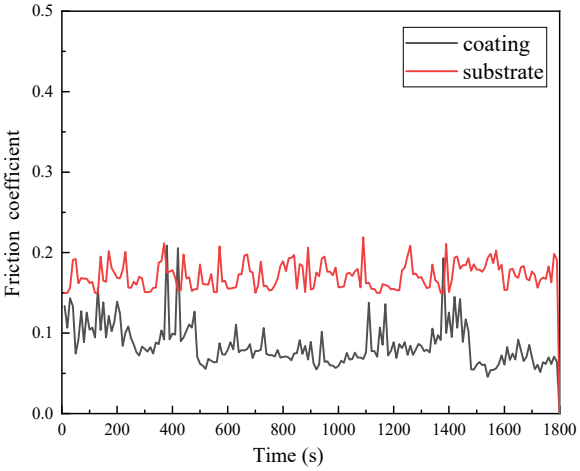

Figure 9. Friction coefficient of Ni60-WC coating.

Table 5 includes the wear rate of the Ni60-WC coating and copper substrate. The wear rate of the Ni60-WC coating is 4.9×10^{-5} $mm^3 \cdot N^{-1} \cdot m^{-1}$, which is only 1.14% of the rate of copper substrate (4.3×10^{-3} $mm^3 \cdot N^{-1} \cdot m^{-1}$). It indicates that the Ni60-WC coating has a better friction and wear property. Figure 10 depicts the morphology of wear for the cladding coating. There were many small ploughs on the surface of Ni60-WC coating, which was a type of abrasive wear.

Table 5. Wear rate of the copper substrate and Ni60-WC coating.

Item	Wear Rate ($mm^3 \cdot N^{-1} \cdot m^{-1}$)
Copper substrate	4.3×10^{-3}
Ni60-WC coating	0.049×10^{-3}

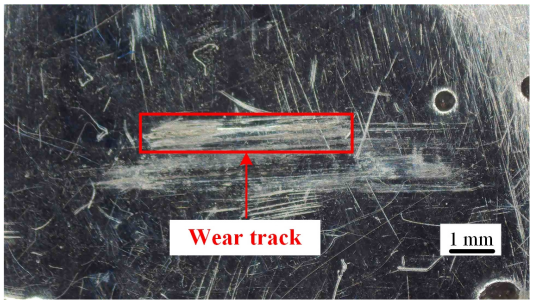

Figure 10. Wear tracks of Ni60-WC coating.

3.5. Corrosion Resistance

Figure 11 shows the polarization curves of the Ni60-WC coating's surface and substrate. It can be seen that the polarization curves of the coating and substrate have the same trend, which presents a certain passivation behavior. The open circuit potential and the minimum corrosion current density of Ni60-WC coating are −0.708 V and 2.34×10^{-7} mA·mm^{-2}, respectively. The corrosion current density of Ni60-WC coating is lower than that of the substrate (1.14×10^{-6} mA·mm^{-2}). The reason is that the appearance of Cr_7C_3 phase improves the corrosion resistance of the Ni60-WC coating.

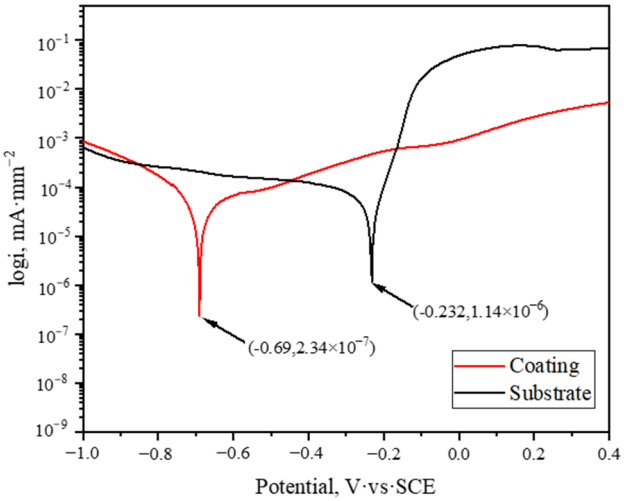

Figure 11. Polarization curve of coating's surface and substrate in 3.5 wt.% NaCl solution.

Table 6 describes electrochemical experimental data of the coating and substrate. According to the Tafel extrapolation method, the anode/cathode Tafel slopes (β_a and β_c) are obtained from the intersection of the tangents of the cathode and anode Tafel curves [32]. The corrosion rate (r_{corr}) and polarization resistance (R_p) are calculated by the Equations (1) and (2).

$$r_{corr} = 0.00327 \times \frac{i_{corr} \times M}{d} \quad (1)$$

$$R_p = \frac{\beta_a \times \beta_c}{2.303 \times i_{corr} \times (\beta_a + \beta_c)} \quad (2)$$

where M is the equivalent weight and d is the density of the simple.

Table 6. The corresponding electrochemical parameters of the laser cladded coatings.

Item	E_{corr} (V)	$i_{corr} \times 10^6$ (mA·mm^{-2})	β_a (mV·dec^{-1})	β_c (mV·dec^{-1})	Rp (kΩ)	Corrosion Rate ((mm/year) × 10^2)
Ni60-WC coating	−0.69	0.234	59.8	−160.1	113.74	1.58
Copper substrate	−0.232	1.14	37.5	−123.979	33.9	1.83

According to the value of Tafel slope, the absolute value of β_a of the Ni60-WC coating is less than the absolute value of β_c, indicating that the corrosion process is under cathodic control. Copper alloy substrate has the same trend. Therefore, the corrosion is controlled by charge transfer at the open circuit potential. The polarization resistance of the coating is 113.74 kΩ, which is higher than the 33.9 kΩ polarization resistance of the substrate, which proves that the corrosion resistance of the coating is better than that of the substrate.

The corrosion mechanism of copper alloy is shown in Figure 12a. The passive film on the surface of copper alloy during corrosion can improve its corrosion resistance. However, the passive film in the presence of corrosive ions (such as Cl^- ions) environment will be completely destroyed, which could result in corrosion of copper alloys. As shown in Figure 12a, Cl^- ions are adsorbed on the surface of the passive film and reducing the protective effect of oxygen on the passive film [33]. In addition, Cl^- ions are transferable in the passive film. When Cl^- ions migrate to the interface between copper and passive film, passive film will be destroyed, as shown in Figure 12a. Cl^- ions are adsorbed at the defects on the copper alloy, resulting in further erosion.

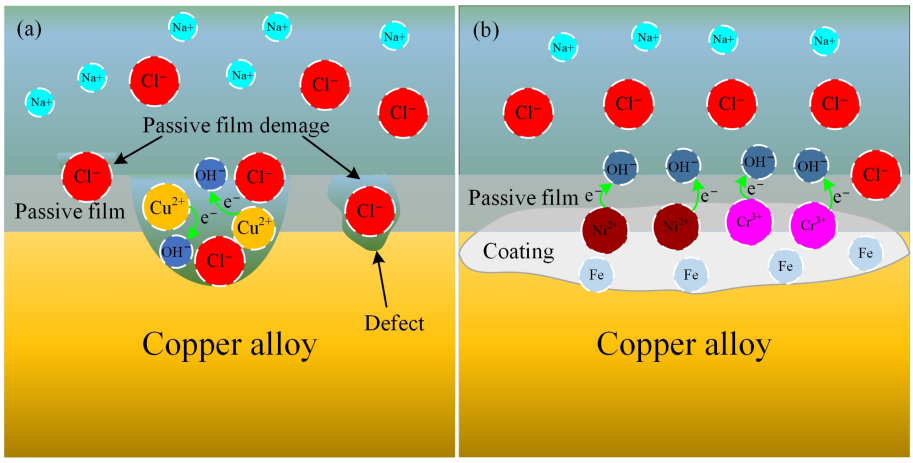

Figure 12. The corrosion mechanism schematic diagram of (**a**) copper alloy and (**b**) Ni60-WC coating.

The anti-corrosion mechanism of the Ni60-WC coating is shown in Figure 12b. Ni-based coating can inhibit the penetration of water and corrosive Cl^- ions, thus isolating the corrosive media and copper alloy contact, so that the corrosion reaction is difficult to occur. The NaCl corrosion solution is a neutral corrosion solution. In this environment, the γ (Fe, Ni) phase is used as the anode during the electrode reaction, and the oxygen evolution corrosion mainly occurs of reaction (3) to (5):

$$\text{Anodic reaction: } Ni - 2e^- \rightarrow Ni^{2+} \quad (3)$$

$$\text{Cathodic reaction: } O^2 + 4e^- + 2H_2O \rightarrow 4OH^- \quad (4)$$

$$\text{Overall reaction: } 2Ni + O^2 + 2H_2O \rightarrow 2Ni(OH)_2 \quad (5)$$

Although the coating is protected on the surface of the copper alloy, small corrosion pits will appear as the corrosion time increases because of the corrosion of the Ni atoms in the γ (Fe, Ni) phase. However, the structure of the coating is uniform and dense, which

inhibits its oxidation activity. At the same time, due to the existence of Cr element in Ni60-WC coating, the Cr element is involved in corrosion and dissolution reaction occurs of reaction (6) to (8):

$$\text{Anodic reaction: } Cr - 3e^- \rightarrow Cr^{3+} \quad (6)$$

$$\text{Cathodic reaction: } O^2 + 4e^- + 2H_2O \rightarrow 4OH^- \quad (7)$$

$$\text{Overall reaction: } 4Cr + 3O^2 + 6H_2O \rightarrow 4Cr(OH)_3 \quad (8)$$

With the increase of the dynamic potential, the dissolution rate of the anode current and the formation rate of the passive film reach a steady state, and the passive interval appears on the polarization curve, and the passive reaction occurs by of reaction (9) to (10):

$$Ni(OH)_2 \rightarrow NiO + H_2O \quad (9)$$

$$2Cr(OH)_3 \rightarrow Cr2O3 + 3H_2O \quad (10)$$

Therefore, NiO and Cr_2O_3 form in the passive film. When the corrosion potential increases to the pitting potential, the anode potential increases rapidly and the transpassivation occurs of reaction (11) to (12):

$$NiO + 2Cl^- + 2H^+ \rightarrow NiCl_2 + 2H_2O \quad (11)$$

$$Cr_2O_3 + 6H^+ + 6Cl^- \rightarrow 2CrCl_3 + 3H_2O \quad (12)$$

On the one hand, Ni and Cr atoms adsorbs more Cl^- ions than the copper substrate and the passive film formed by the oxides of Ni and Cr have better corrosion resistance than the passive film formed by the oxides of copper. On the other hand, due to the inhomogeneity of electrochemical corrosion in the grain boundary and grain interior of copper, new phases are precipitated at the grain boundary of copper. This will lead to intergranular corrosion, so that the passive film may be weakened in different properties and reduce the corrosion performance of copper alloy [34]. Overall, the corrosion resistance of the Ni60-WC coating is better than that of copper alloy.

Figure 13 describes the morphology of the cladding coating after electrochemical corrosion. In the middle of cladding coating, refined dendritic region is corroded, while the inter dendritic region has small change. The reason is that the central refined dendritic region is mainly composed of γ (Fe, Ni) phase. In the corrosion process, the Fe atoms are easy to participate in the oxidation reaction, resulting in serious corrosion.

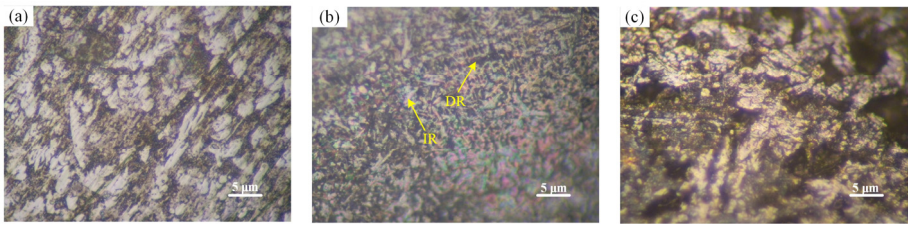

Figure 13. The morphology of cladding coating after electrochemical corrosion: (**a**) outermost surface; (**b**) middle; and (**c**) binding region.

4. Conclusions

In this study, the following conclusions are drawn:

(1) A Ni60-WC coating is successfully fabricated on the preheated copper substrate by laser. The cladding coating is composed of some reinforced phases, such as γ (Fe, Ni), M_7C_3, WC and $Cr_{0.09}Fe_{0.7}Ni_{0.21}$.

(2) The average microhardness is 941.6 $HV_{0.5}$, which is about 4.7 times greater than that of copper alloy substrate.

(3) The wear rate of the cladding coating is 4.9×10^{-5} $mm^3 \cdot N^{-1} \cdot m^{-1}$, which was about 1.14% of copper substrate. The existence of the reinforced phases decreases the friction coefficient and improves the wear resistance of the copper substrate.
(4) The open circuit potential and the minimum corrosion current density of the Ni60-WC coating are −0.708 V and 2.34×10^{-7} $mA \cdot mm^{-2}$, respectively. The Ni60-WC coating exhibits excellent corrosion resistance compared with copper alloy.

Author Contributions: Conceptualization, Y.L.; data curation, Y.L.; formal analysis, T.X. and G.L.; funding acquisition, Y.L.; methodology, T.X. All authors have read and agreed to the published version of the manuscript.

Funding: This research was funded by the National Natural Science Foundation of China (51704073), Jilin Province Science and Technology Development (20180520065JH), Jilin Province "13th Five-Year Plan" Science and Technology Research Project of Education Department (JJKH20180419KJ/JJKH20180427KJ), and Jilin City Technology Innovation Development Project (20166013).

Institutional Review Board Statement: Not applicable.

Informed Consent Statement: Not applicable.

Data Availability Statement: Not applicable.

Conflicts of Interest: The authors declare no conflict of interest.

References

1. Wang, Y.; Zhuo, L.; Yin, E. Progress, challenges and potentials/trends of tungsten-copper (W-Cu) composites/pseudo-alloys: Fabrication, regulation and application. *Int. J. Refract. Met. Hard Mater.* **2021**, *100*, 105648. [CrossRef]
2. Ebrahimi, M.; Par, M.A. Twenty-year uninterrupted endeavor of friction stir processing by focusing on copper and its alloys. *J. Alloys Compd.* **2019**, *781*, 1074–1090. [CrossRef]
3. Zhang, H.; Fu, H.; Zhu, S.; Yong, W.; Xie, J. Machine learning assisted composition effective design for precipitation strengthened copper alloys. *Acta Mater.* **2021**, *215*, 117118. [CrossRef]
4. Kuanyshev, M.; Nuralin, B.; Salimov, B.; Kaukarov, A.; Murzagaliev, A.; Narikov, K.; Shakeshev, B. The improvement of friction bearing manufacturing technology by using cop-per alloy. *Int. J. Adv. Manuf. Technol.* **2017**, *88*, 317–324. [CrossRef]
5. Liu, Y.; Xu, T.; Liu, Y.; Gao, Y.L.; Di, C. Wear and heat shock resistance of Ni-WC coating on mould copper plate fabricated by laser. *J. Mater. Res. Technol.* **2020**, *9*, 8283–8288. [CrossRef]
6. Fuseini, M.; Zaghloul, M.M.Y. Investigation of Electrophoretic Deposition of PANI Nano fibers as a Manufacturing Technol-ogy for corrosion protection. *Prog. Org. Coat.* **2022**, *171*, 107015. [CrossRef]
7. Abedini, B.; Ahmadi, N.P.; Yazdani, S.; Magagnin, L. Electrodeposition and corrosion behavior of Zn-Ni-Mn alloy coatings deposited from alkaline solution. *Trans. Nonferr. Met. Soc. China* **2020**, *30*, 548–558. [CrossRef]
8. Zang, J.; Li, H.; Sun, J.; Shen, Y.; Su, N.; Feng, X. Microstructure and thermal conductivity of Cu-Cu_2AlNiZnAg/diamond coatings on pure copper substrate via high-energy mechanical alloying method. *Surf. Interfaces* **2020**, *21*, 100742. [CrossRef]
9. Li, Z.; Yan, H.; Zhang, P.; Guo, J.; Yu, Z.; Ringsberg, J.W. Improving surface resistance to wear and corrosion of nickel-aluminum bronze by laser-clad TaC/Co-based alloy composite coatings. *Surf. Coat. Technol.* **2021**, *405*, 126592. [CrossRef]
10. Scendo, M.; Staszewska-Samson, K.; Danielewski, H. Corrosion Behavior of Inconel 625 Coating Produced by Laser Cladding. *Coatings* **2021**, *11*, 759. [CrossRef]
11. Chen, W.; Chen, Q.; Zhang, Z.; Tang, S.; Cai, Q. Microstructure and Fatigue of EA4T Steel in Laser Cladding Remanufacturing. *Coatings* **2022**, *12*, 1106. [CrossRef]
12. Hu, Z.; Li, Y.; Lu, B.; Tan, N.; Cai, L.; Yong, Q. Effect of WC content on microstructure and properties of high-speed laser cladding Ni-based coating. *Opt. Laser Technol.* **2022**, *155*, 108449. [CrossRef]
13. Sun, M.; Pang, M. Defect Formation Mechanism and Performance Study of Laser Cladding Ni/Mo Composite Coating. *Coatings* **2021**, *11*, 1460. [CrossRef]
14. Jin, L.; Jiang, K.; Kang, L.; Yan, B. Laser Cladding on Copper with Composite Powder C-Al2O3-Cu. *J. Mater. Eng. Perform.* **2022**, *31*, 1317–1324. [CrossRef]
15. Yin, J.; Wang, D.; Meng, L.; Ke, L.; Hu, Q.; Zeng, X. High-temperature slide wear of Ni-Cr-Si metal silicide based composite coatings on copper substrate by laser-induction hybrid cladding. *Surf. Coat. Technol.* **2017**, *325*, 120–126. [CrossRef]
16. Lu, S.; Wang, L.; Zhou, J.; Liang, J. Microstructure and tribological properties of laser-cladded Co-Ti3SiC2 coating with Ni-based interlayer on copper alloy. *Tribol. Int.* **2022**, *171*, 107549. [CrossRef]
17. Pellizzari, M.; Zhao, Z.; Bosetti, P.; Perini, M. Optimizing direct laser metal deposition of H13 cladding on CuBe alloy sub-strate. *Surf. Coat. Tech.* **2022**, *432*, 128084. [CrossRef]

18. Wang, N.; Yu, H.; Zhao, P.; Zhang, J.-M.; Gong, J.-G.; Xuan, F.-Z. Cyclic deformation response of austenitic Ni-based alloy: Mechanical behavior, internal stress evolution and microstructural feature. *Mater. Sci. Eng. A* **2022**, *850*, 143522. [CrossRef]
19. Wan, Z.; Dai, W.; Guo, W.; Jia, Q.; Zhang, H.; Xue, J.; Lin, L.; Peng, P. Improved corrosion resistance of Ni-base Al-loy 600 welded joint by laser shock peening. *J. Manuf. Process.* **2022**, *80*, 718–728. [CrossRef]
20. Bhaskararao, K.A.; Janardhana, G.R. Influence of Al_2O_3 and ZrO_2 alloying on microstructure, hardness and flexural strength of Ni based functionally graded composites by vacuum sintering. *Compos. Commun.* **2020**, *22*, 100458. [CrossRef]
21. Wang, Q.; Zhai, L.L.; Zhang, L.; Zhang, J.W.; Ban, C.Y. Effect of steady magnetic field on microstructure and properties of laser cladding Ni-based alloy coating. *J. Mater. Res. Technol.* **2022**, *17*, 2145–2157. [CrossRef]
22. Feng, X.; Wang, H.; Liu, X.; Wang, C.; Cui, H.; Song, Q.; Huang, K.; Li, N.; Jiang, X. Effect of Al content on wear and corrosion resistance of Ni-based alloy coatings by laser cladding. *Surf. Coat. Tech.* **2021**, *412*, 126976. [CrossRef]
23. García, A.; Fernández, M.R.; Cuetos, J.M.; González, R.; Ortiz, A.; Cadenas, M. Study of the Sliding Wear and Friction Behavior of WC + NiCrBSi Laser Cladding Coatings as a Function of Actual Concentration of WC Reinforcement Particles in Ball-on-Disk Test. *Tribol. Lett.* **2016**, *63*, 1–10. [CrossRef]
24. Zhang, P.-X.; Yan, H.; Sun, Y.-H. Microstructure, microhardness and corrosion resistance of laser cladding Al_2O_3@Ni composite coating on 304 stainless steel. *J. Mater. Sci.* **2021**, *56*, 8209–8224. [CrossRef]
25. Zhao, Y.; Yu, T.; Sun, J.; Jiang, S. Microstructure and properties of laser cladded B_4C/TiC/Ni-based composite coating. *Int. J Refract. Met. Hard Mater.* **2020**, *86*, 105112. [CrossRef]
26. Su, W.; Cui, X.; Yang, Y.; Guan, Y.; Zhao, Y.; Wan, S.; Li, J.; Jin, G. Effect of Si content on microstructure and tribological properties of Ti_5Si_3/TiC reinforced NiTi laser cladding coatings. *Surf. Coat. Technol.* **2021**, *418*, 127281. [CrossRef]
27. Tang, B.; Tan, Y.; Zhang, Z.; Xu, T.; Sun, Z.; Li, X. Effects of Process Parameters on Geometrical Characteristics, Microstructure and Tribological Properties of TiB_2 Reinforced Inconel 718 Alloy Composite Coatings by Laser Cladding. *Coatings* **2020**, *10*, 76. [CrossRef]
28. Jiang, J.; Pang, X.; Zhou, J.; Li, B.; Zhou, F. Optical performance and corrosion resistance of TiN/Ni multiphase cermet by laser cladding. *Opt. Laser Technol.* **2021**, *143*, 107308. [CrossRef]
29. Zhao, S.; Yang, L.; Huang, Y.; Xu, S. A novel method to fabricate Ni/WC composite coatings by laser wire deposition: Processing characteristics, microstructural evolution and mechanical properties under different wire transfer modes. *Addit. Manuf.* **2021**, *38*, 101738. [CrossRef]
30. Wang, H.; Sun, Y.; Qiao, Y.; Du, X. Effect of Ni-coated WC reinforced particles on microstructure and mechanical properties of laser cladding Fe-Co duplex coating. *Opt. Laser Technol.* **2021**, *142*, 107209. [CrossRef]
31. Shen, S.; He, X.; Gao, L.; Su, G.; Xu, C.; Xu, N. Study on crack behavior of laser cladding ceramic-metal composite coating with high content of WC. *Ceram. Int.* **2022**, *48*, 17460–17470. [CrossRef]
32. Farahmand, P.; Kovacevic, R. Corrosion and wear behavior of laser cladded Ni–WC coatings. *Surf. Coat. Technol.* **2015**, *276*, 121–135. [CrossRef]
33. Uhlig, H.H. Adsorbed and reaction-produce films onmetals. *J. Electrochem. Soc.* **1950**, *97*, 215C–220C. [CrossRef]
34. Wu, L.; Ma, A.; Zhang, L.; Zheng, Y. Intergranular erosion corrosion of pure copper tube in flowing NaCl solution. *Corros. Sci.* **2022**, *201*, 110304. [CrossRef]